The Astrophysical Journal, 835:189 (7pp), 2017 February 1 doi:10.3847/1538-4357/835/2/189

KIC 11401845: An Eclipsing Binary with Multiperiodic Pulsations and Light-travel Time

Jae Woo Lee[1,2], Kyeongsoo Hong[1], Seung-Lee Kim[1,2], and Jae-Rim Koo[1]
[1] Korea Astronomy and Space Science Institute, Daejeon 34055, Korea; jwlee@kasi.re.kr, kshong@kasi.re.kr
[2] Astronomy and Space Science Major, Korea University of Science and Technology, Daejeon 34113, Korea; slkim@kasi.re.kr, koojr@kasi.re.kr
Received 2016 November 22; revised 2016 December 27; accepted 2016 December 29; published 2017 January 31

Abstract

We report the *Kepler* photometry of KIC 11401845 displaying multiperiodic pulsations, superimposed on binary effects. Light-curve synthesis shows that the binary star is a short-period detached system with a very low mass ratio of $q = 0.070$ and filling factors of $F_1 = 45\%$ and $F_2 = 99\%$. Multiple-frequency analyses were applied to the light residuals after subtracting the synthetic eclipsing curve from the observed data. We detected 23 frequencies with signal-to-noise ratios larger than 4.0, of which the orbital harmonics (f_4, f_6, f_9, f_{15}) in the low-frequency domain may originate from tidally excited modes. For the high frequencies of 13.7–23.8 day^{-1}, the period ratios and pulsation constants are in the ranges of $P_{\rm pul}/P_{\rm orb} = 0.020$–$0.034$ and $Q = 0.018$–0.031 days, respectively. These values and the position on the Hertzsprung–Russell diagram demonstrate that the primary component is a δ Sct pulsating star. We examined the eclipse timing variation of KIC 11401845 from the pulsation-subtracted data and found a delay of 56 ± 17 s in the arrival times of the secondary eclipses relative to the primary eclipses. A possible explanation of the time shift may be some combination of a light-travel-time delay of about 34 s and a very small eccentricity of $e\cos\omega < 0.0002$. This result represents the first measurement of the Rømer delay in noncompact binaries.

Key words: binaries: eclipsing – stars: fundamental parameters – stars: individual (KIC 11401845) – stars: oscillations (including pulsations)

Supporting material: machine-readable table

1. Introduction

The *Kepler* satellite provides the highly precise and nearly continuous photometric data for ~200,000 objects that have helped to revolutionize the study of stars themselves, as well as extrasolar planets (Borucki et al. 2010; Koch et al. 2010). There are 2878 eclipsing and ellipsoidal binaries in the *Kepler* main field of view (Kirk et al. 2016), corresponding to about 1.3% of all observed targets. Eclipsing binaries (EBs) serve as critical tools that provide an accurate and direct determination of fundamental stellar parameters such as the mass and radius for each component. These data allow us to test stellar evolution models and to determine distances of binary systems (Torres et al. 2010). Furthermore, it is possible to measure precisely mid-eclipse times from binary light curves. The timing measurements are used to investigate a variety of physical phenomena causing the orbital period changes of EBs (Hilditch 2001; Kreiner et al. 2001). Such examples are mass transfer, angular momentum loss, apsidal motion in an elliptical orbit, the third-body effect, and magnetic activity cycle.

EBs with pulsating components are very promising objects for the study of stellar structure and evolution, because binarity provides useful information about the components and asteroseismology assists in probing the interiors of stars. Most of them have been found to be δ Sct-type pulsators of classical semidetached Algols (Mkrtichian et al. 2004; Liakos & Niarchos 2017). The δ Sct stars are dwarfs and subgiants with spectral types A and F located in the lower portion of the Cepheid instability strip. They pulsate in low-order pressure (p) modes with typical periods of 0.02–0.25 days and amplitudes of less than 0.1 mag (Breger 2000; Rodríguez & Breger 2001). The pulsations are driven by the κ mechanism, mostly due to partial ionization of He II. The δ Sct variables in binaries have pulsation features similar to single δ Sct stars, but their pulsations can be affected by mass transfer between both components and gravitation forces from companions. Recently, Liakos & Niarchos (2015, 2016) showed that there is a threshold in the orbital period of ~13 days below which the pulsations are influenced by the binarity. In eccentric-orbit binaries, some pulsations can be excited by tidal interaction. The signature of the tidally excited modes are the frequencies at multiples of the orbital frequency (Welsh et al. 2011; Hambleton et al. 2013).

This paper is the fifth contribution in a series of detailed studies for pulsating stars in the *Kepler* EBs (Lee et al. 2014, 2016a, 2016b; Lee 2016). We present that KIC 11401845 (R.A.$_{2000} = 19^{\rm h}25^{\rm m}11\overset{\rm s}{.}275$; decl.$_{2000} = +49°14'40\overset{''}{.}09$; $K_{\rm p} = +14.355$; $g = +14.443$; $g - r = +0.118$) is a detached EB exhibiting multiperiodic pulsations and light-travel-time (LTT) delay. The system was announced to be an EB pulsating at frequencies of 13–25 day^{-1} by Gaulme & Guzik (2014).

2. *Kepler* Photometry and Light-curve Synthesis

The *Kepler* data of KIC 11401845 were obtained in a long-cadence mode of 29.42 minutes during Quarters 10 and 12. We used the Simple Aperture Photometry (SAP) time-series data in Data Release 25 retrieved from the *Kepler* Data Archive.[3] The raw data were detrended by using second-order polynomials that were separately applied to each quarter. As eclipses influence the detrending process, we fitted the polynomial to only the outside-eclipse part of the light curve (e.g., Hambleton et al. 2013). The flux measurements were converted to a magnitude scale by requiring a *Kepler* magnitude of +14.355 at maximum light. The detrended *Kepler* data are displayed in

[3] http://archive.stsci.edu/kepler/

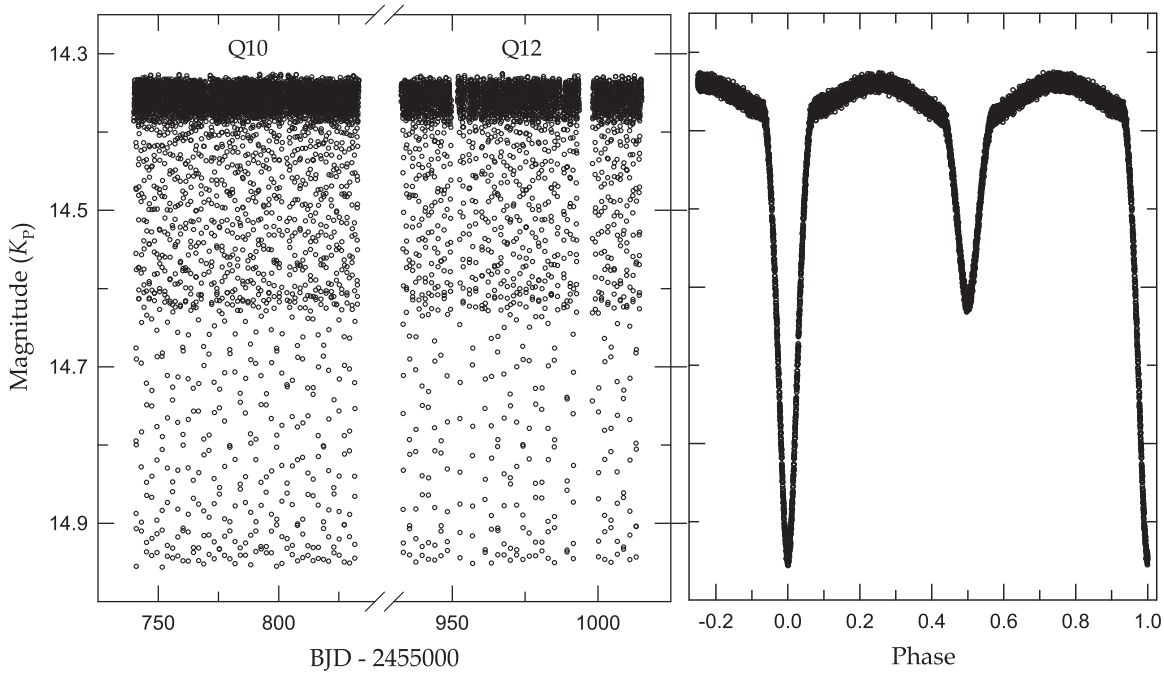

Figure 1. Detrended *Kepler* data of KIC 11401845 distributed in BJD (left panel) and orbital phase (right panel).

Table 1
Binary Parameters of KIC 11401845

Parameter	Model 1[a]		Model 2[b]	
	Primary	Secondary	Primary	Secondary
T_0 (BJD)	2,455,740.80720(13)		2,455,740.80729(5)	
P (days)	2.1613895(18)		2.1613910(6)	
q	0.0699(16)		0.0695(10)	
i (deg)	85.45(21)		85.10(12)	
T (K)	7590	6217(26)	7590	6154(19)
Ω	4.150(29)	1.879(7)	4.138(21)	1.873(4)
Ω_{in}	1.861		1.860	
A	1.0	0.5	1.0	0.5
g	1.0	0.32	1.0	0.32
X, Y	0.671, 0.199	0.632, 0.232	0.671, 0.199	0.633, 0.229
x, y	0.599, 0.238	0.629, 0.280	0.599, 0.238	0.633, 0.278
$L/(L_1+L_2)$	0.7905(12)	0.2095	0.7940(8)	0.2060
r (pole)	0.2450(13)	0.1638(29)	0.2457(10)	0.1651(19)
r (point)	0.2474(14)	0.2083(78)	0.2481(10)	0.2136(56)
r (side)	0.2470(14)	0.1695(32)	0.2476(10)	0.1710(21)
r (back)	0.2473(14)	0.1928(49)	0.2480(10)	0.1956(32)
r (volume)[c]	0.2464(14)	0.1753(43)	0.2471(10)	0.1771(29)
$\sum W(O-C)^2$	0.0050		0.0016	
Absolute parameters:				
M ($M_\odot$)	1.70(8)	0.119(7)	1.70(8)	0.118(6)
R ($R_\odot$)	2.11(5)	1.50(5)	2.12(4)	1.52(4)
log g (cgs)	4.02(3)	3.16(4)	4.02(3)	3.15(3)
L ($L_\odot$)	13(2)	3.0(4)	13(2)	3.0(4)
M_{bol} (mag)	1.92(12)	3.53(16)	1.92(12)	3.55(15)
BC (mag)	0.03(1)	−0.02(2)	0.03(1)	−0.03(2)
M_V (mag)	1.89(12)	3.55(16)	1.89(12)	3.58(15)

Notes.
[a] Result from the observed data.
[b] Result from the pulsation-subtracted data.
[c] Mean volume radius.

Figure 1. The shape of the light curve indicates a significant temperature difference between the binary components and an ellipsoidal variation due to tidal distortions.

To derive the binary parameters of this system, all *Kepler* data were analyzed using the Wilson–Devinney binary program (Wilson & Devinney 1971; Van Hamme & Wilson 2007; hereafter W–D). This synthesis was performed in a way similar to that for the pulsating EBs V404 Lyr (Lee et al. 2014) and KIC 6220497 (Lee et al. 2016a). The effective temperature of the hotter and more massive star was set to be 7590 K from the *Kepler* Input Catalog (KIC; Kepler Mission Team 2009). The logarithmic bolometric ($X_{1,2}$) and monochromatic ($x_{1,2}$) limb-darkening coefficients were interpolated from the values of Van Hamme (1993). In Table 1, the parentheses signify the adjusted parameters. In this article, the subscripts 1 and 2 refer to the primary and secondary components being eclipsed at orbital phases 0.0 (Min I) and 0.5 (Min II), respectively.

There has been neither a light-curve solution nor a spectroscopic mass ratio (q) for KIC 11401845 so far. Thus, we conducted a photometric q-search procedure that calculates a series of models with varying q from 0 to 1. For each assumed mass ratio, the W–D code was applied for various modes but converged satisfactorily only when detached mode 2 was used. The weighted sum of the squared residuals, $\sum W(O-C)^2$, reached a minimum around $q = 0.07$, which was adopted as the initial value and thereafter adjusted to derive the photometric solutions. The result is given as Model 1 in the second and third columns of Table 1. The synthetic light curve appears as the blue solid curve in Figure 1, and the corresponding light residuals are plotted as the gray crosses in the figure. In all the procedures, we considered an orbital eccentricity (e) and a third light (l_3) as additional free parameters. Both searches led to values for the two parameters that were zero within their errors, which implies that KIC 11401845 has negligible eccentricity. We obtained the errors for the adjustable parameters by splitting the *Kepler* data into 79 segments at intervals of an orbital period and analyzing them separately (Koo et al. 2014). In Table 1, the error of each parameter is its standard deviation computed from this process.

Absolute parameters for KIC 11401845 can be computed from our light-curve solutions in Table 1 and from the correlations between spectral type (temperature) and stellar mass. The surface temperature ($T_1 = 7590$ K) of the primary star corresponds to a normal dwarf one with a spectral type of ~A8V. Assuming that each component has a temperature error of 200 K, the primary's mass was estimated to be $M_1 = 1.70 \pm 0.08\,M_\odot$ from Harmanec's (1988) empirical relation. We calculated the absolute dimensions for each component given in the last part of Table 1. Here, the luminosity (L) and bolometric magnitudes ($M_{\rm bol}$) were derived by using $T_{\rm eff\odot} = 5780$ K and $M_{\rm bol\odot} = +4.73$. The bolometric corrections (BCs) were obtained from the expression between $\log T_{\rm eff}$ and BC given by Torres (2010).

Considering the temperature error of the primary star, we carried out the light-curve synthesis for 7390 and 7790 K. The binary parameters from the two limits are in satisfactory agreement with those from $T_1 = 7590$ K, except for the secondary's temperature (T_2). In the three models, the temperature ratios (T_2/T_1) of both components are consistent with each other within their errors. We can see that the adopted T_1 does not affect the results presented in this paper.

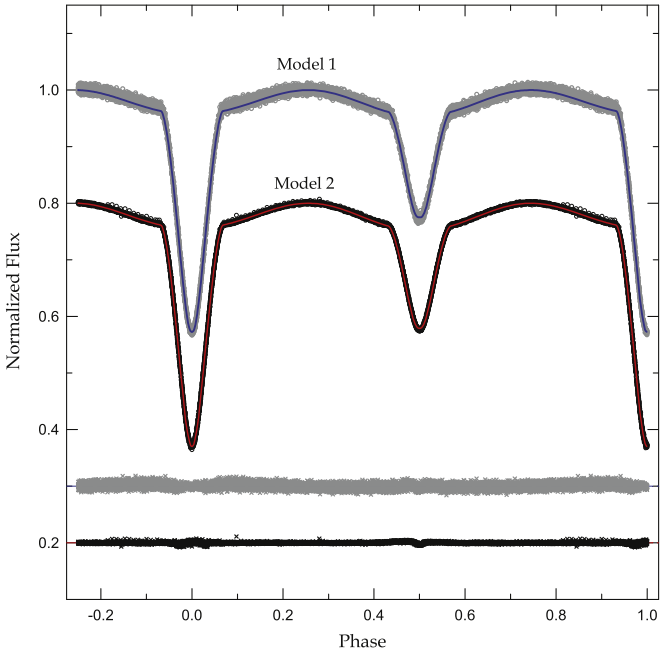

Figure 2. Binary light curve before (gray circles) and after (black circles) subtracting the pulsation signatures from the *Kepler* data. The blue and red solid curves are computed with the Model 1 and Model 2 parameters of Table 1, respectively. The corresponding residuals from the fits are offset from zero and plotted at the bottom in the same order as the light curves. In the light residuals from Model 2, some feature is certainly visible during the times of the secondary eclipse, which may come from insufficient removal of the pulsation effects in the orbital phases.

3. Light Residuals and Pulsational Characteristics

From the temperature (T_1) and surface gravity ($\log g_1$) given in Table 1, the primary star of KIC 11401845 resides within the δ Sct instability strip; hence, it would be a candidate for δ Sct pulsations. For more reliable frequency analysis, we followed the procedure described by Lee (2016). First, we divided the observed *Kepler* data of KIC 11401845 into 79 subsets as before and modeled each light curve with the W–D code by adjusting only the ephemeris epoch (T_0) in Model 1 of Table 1. Second, the corresponding residuals from the entire data sets were applied to multiple-frequency analyses in the range from 0 to the Nyquist limit of $f_{\rm Ny} = 24.4$ day^{-1} using the PERIOD04 program (Lenz & Breger 2005). Because the binary components block each other's lights during eclipses, we used only the outside-eclipse residuals (orbital phases 0.07–0.43 and 0.57–0.93). According to the successive prewhitening procedures, we detected the frequencies with signal-to-noise ratios (S/Ns) larger than 4.0 (Breger et al. 1993). Third, we solved the pulsation-subtracted data after removing the pulsations from the observed data. As a result, new binary parameters were obtained, and they were used to reanalyze the 79 light curves in the first stage.

This process was repeated three times until the detected frequencies were unchanged. Final binary parameters are given as Model 2 in the fourth and fifth columns of Table 1, and the pulsation-subtracted data and model light curve are plotted in Figure 2. We can see that the physical parameters for Model 2 are consistent with those for Model 1. Figure 3 shows the light residuals after removal of the binary effects from the observed *Kepler* data. We detected a total of 23 frequencies larger than the empirical threshold of S/N = 4.0.

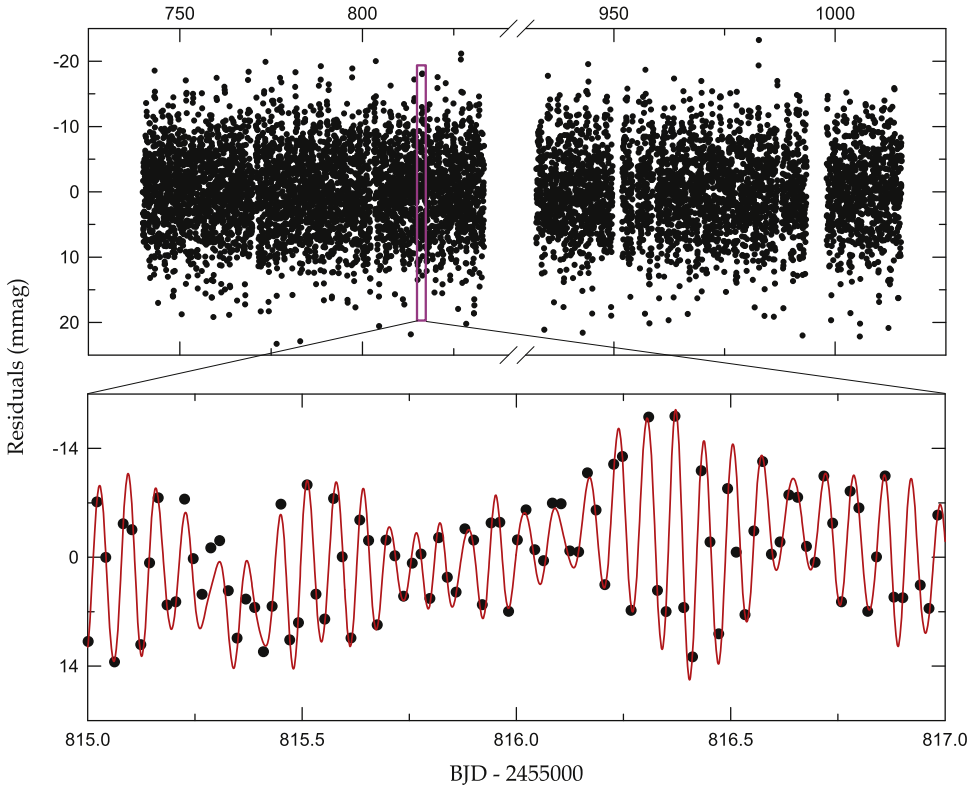

Figure 3. Light residuals after removing the binarity effects from the *Kepler* light curve. The bottom panel presents a short section of the residuals marked by the inset box in the top panel. The synthetic curve is computed from the 23-frequency fit to the data.

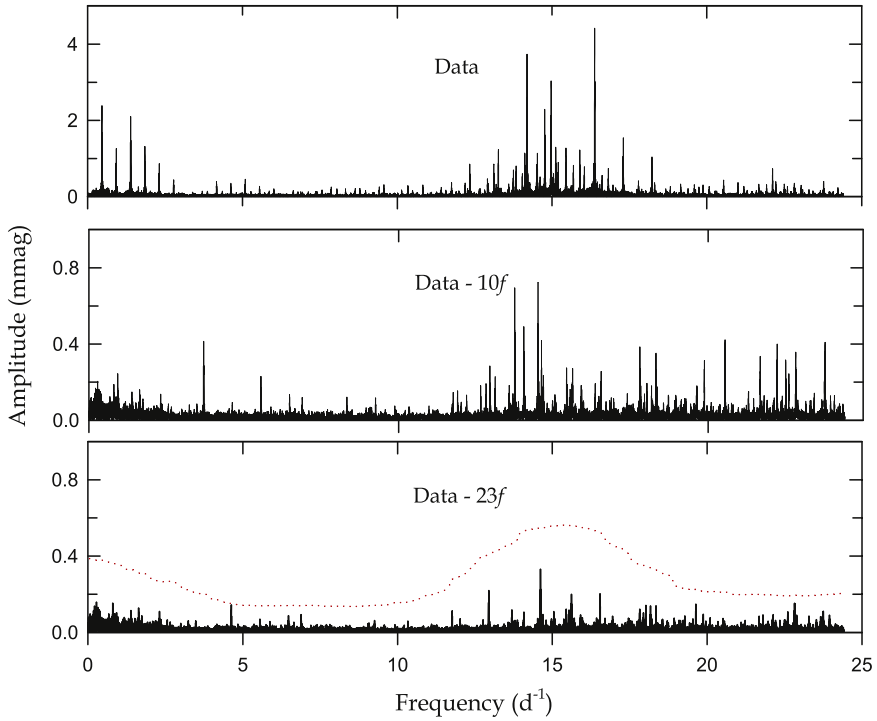

Figure 4. Amplitude spectra before (top panel) and after prewhitening the first 10 frequencies (middle panel) and all 23 frequencies (bottom panel) from the PERIOD04 program for all of the outside-eclipse residual data. The dotted line in the bottom panel corresponds to four times the noise spectrum, which was calculated for each frequency in an equidistant step of 0.1 day^{-1}.

The amplitude spectra before and after prewhitening the first 10 frequencies and then all 23 frequencies are shown in the top to bottom panels of Figure 4, respectively. The detailed result from the frequency analysis is listed in Table 2, where the frequencies are given in order of detection and the noises are calculated in the range of 5 day^{-1} around each frequency. The uncertainties in the table were obtained according to Kallinger et al. (2008). The synthetic curve computed from

Table 2
Multiple-frequency Analysis of KIC 11401845

Designation	Frequency (day^{-1})	Amplitude (mmag)	Phase (rad)	S/N	Q (days)	Remark
f_1	16.37811 ± 0.00004	4.41 ± 0.23	5.74 ± 0.15	33.13	0.026	⋯
f_2	14.19519 ± 0.00004	3.74 ± 0.23	2.06 ± 0.18	27.93	0.030	⋯
f_3	14.97171 ± 0.00005	3.18 ± 0.24	5.18 ± 0.22	22.85	0.028	⋯
f_4	0.46268 ± 0.00003	3.54 ± 0.16	5.73 ± 0.13	37.42	⋯	$f_{\rm orb}$
f_5	14.76672 ± 0.00007	2.28 ± 0.24	2.63 ± 0.30	16.56	0.029	⋯
f_6	1.85072 ± 0.00005	1.81 ± 0.13	5.33 ± 0.21	23.56	⋯	$4f_{\rm orb}$
f_7	14.12286 ± 0.00014	1.17 ± 0.23	3.79 ± 0.57	8.78	0.030	⋯
f_8	15.20396 ± 0.00019	0.90 ± 0.24	4.42 ± 0.78	6.45	0.028	⋯
f_9	2.77609 ± 0.00007	1.11 ± 0.11	0.95 ± 0.30	16.92	⋯	$6f_{\rm orb}$
f_{10}	22.12255 ± 0.00008	0.73 ± 0.08	1.13 ± 0.33	14.99	0.019	⋯
f_{11}	14.50213 ± 0.00023	0.74 ± 0.23	3.76 ± 0.93	5.41	0.029	$3f_3\,2f_8$
f_{12}	13.75268 ± 0.00021	0.69 ± 0.20	3.11 ± 0.85	5.90	0.031	⋯
f_{13}	14.04653 ± 0.00030	0.55 ± 0.23	1.53 ± 1.20	4.16	0.030	$f_3 - 2f_{\rm orb}$
f_{14}	20.54260 ± 0.00016	0.41 ± 0.09	5.00 ± 0.64	7.87	0.021	$f_1 + 9f_{\rm orb}$
f_{15}	3.70145 ± 0.00012	0.52 ± 0.09	2.88 ± 0.48	10.35	⋯	$8f_{\rm orb}$
f_{16}	22.22705 ± 0.00015	0.40 ± 0.08	3.22 ± 0.61	8.18	0.019	$2f_7 - 13f_{\rm orb}$
f_{17}	23.77410 ± 0.00015	0.40 ± 0.08	0.08 ± 0.62	8.11	0.018	⋯
f_{18}	17.79523 ± 0.00029	0.38 ± 0.15	4.34 ± 1.19	4.21	0.024	⋯
f_{19}	22.82621 ± 0.00017	0.36 ± 0.08	3.22 ± 0.68	7.34	0.019	⋯
f_{20}	21.67877 ± 0.00018	0.35 ± 0.08	2.34 ± 0.71	7.03	0.020	⋯
f_{21}	18.31316 ± 0.00030	0.33 ± 0.14	4.19 ± 1.23	4.07	0.023	⋯
f_{22}	22.50255 ± 0.00019	0.31 ± 0.08	6.20 ± 0.77	6.49	0.019	⋯
f_{23}	19.87857 ± 0.00021	0.31 ± 0.09	3.96 ± 0.87	5.79	0.021	⋯

Table 3
Eclipse Timings Measured from Both Data Sets Including and Removing the Pulsations

Observed Data					Pulsation-subtracted Data		
BJD	Error	O–C_1	Epoch	Min	BJD	Error	O–C_2
2,455,740.80714	±0.00031	−0.000150	0.0	I	2,455,740.80719	±0.00014	−0.000100
2,455,741.88860	±0.00120	+0.000615	0.5	II	2,455,741.88849	±0.00028	+0.000504
2,455,742.96856	±0.00064	−0.000121	1.0	I	2,455,742.96867	±0.00039	−0.000011
2,455,744.04971	±0.00083	+0.000334	1.5	II	2,455,744.04989	±0.00031	+0.000514
2,455,745.12985	±0.00038	−0.000222	2.0	I	2,455,745.12994	±0.00025	−0.000132
2,455,746.21091	±0.00064	+0.000142	2.5	II	2,455,746.21106	±0.00020	+0.000293
2,455,747.29119	±0.00050	−0.000273	3.0	I	2,455,747.29126	±0.00020	−0.000203
2,455,748.37248	±0.00162	+0.000322	3.5	II	2,455,748.37242	±0.00034	+0.000262
2,455,749.45263	±0.00030	−0.000224	4.0	I	2,455,749.45265	±0.00028	−0.000204
2,455,750.53383	±0.00052	+0.000281	4.5	II	2,455,750.53397	±0.00019	+0.000421

(This table is available in its entirety in machine-readable form.)

the 23-frequency fit is displayed in the bottom panel of Figure 3.

As listed in Table 2, four in the low-frequency region (0.4–3.8 day^{-1}) and 19 in the high-frequency region (13.7–23.8 day^{-1}) were derived from the multiple-frequency analyses of the outside-eclipse light residuals. Within the frequency resolution of 0.00545 day^{-1} (Loumos & Deeming 1978), we searched the frequencies for possible harmonic and combination terms. The result is given in the last column of Table 2. We think that the f_{11} to f_{23} frequencies mainly arise from combination frequencies, some of which can be caused by imperfect removal of the binary effects in the observed data. On the other hand, the high-frequency signals close to the Nyquist limit can be reflections of real frequencies ($2f_{\rm Ny} - f_i$) higher than $f_{\rm Ny}$ (Murphy et al. 2013; Lee et al. 2016b). High-cadence photometry is needed to separate the Nyquist aliases from the detected frequencies of KIC 11401845.

4. Eclipse Timing Variation and Its Implications

For an orbital period study of KIC 11401845, we determined 150 minimum times and their uncertainties from the observations with the method of Kwee & van Woerden (1956). These minima are listed in columns (1)–(5) of Table 3, where we present the cycle numbers and O–C_1 residuals calculated with the light elements (T_0 and P) for Model 2 in Table 1. The resultant eclipse timing diagram is displayed in the top panel of Figure 5. As shown in the figure, the timing residuals from the primary (filled circle) and secondary (open circle) eclipses do not agree with each other, which could be caused by the light variations due to the multiperiodic pulsations of the primary star. Thus, we recalculated the minimum times from the eclipse light curve after subtracting the 23 frequencies detected in Section 3 from the observed *Kepler* data. The results are given in columns (6)–(8) of Table 3 and are illustrated in the middle panel of Figure 5.

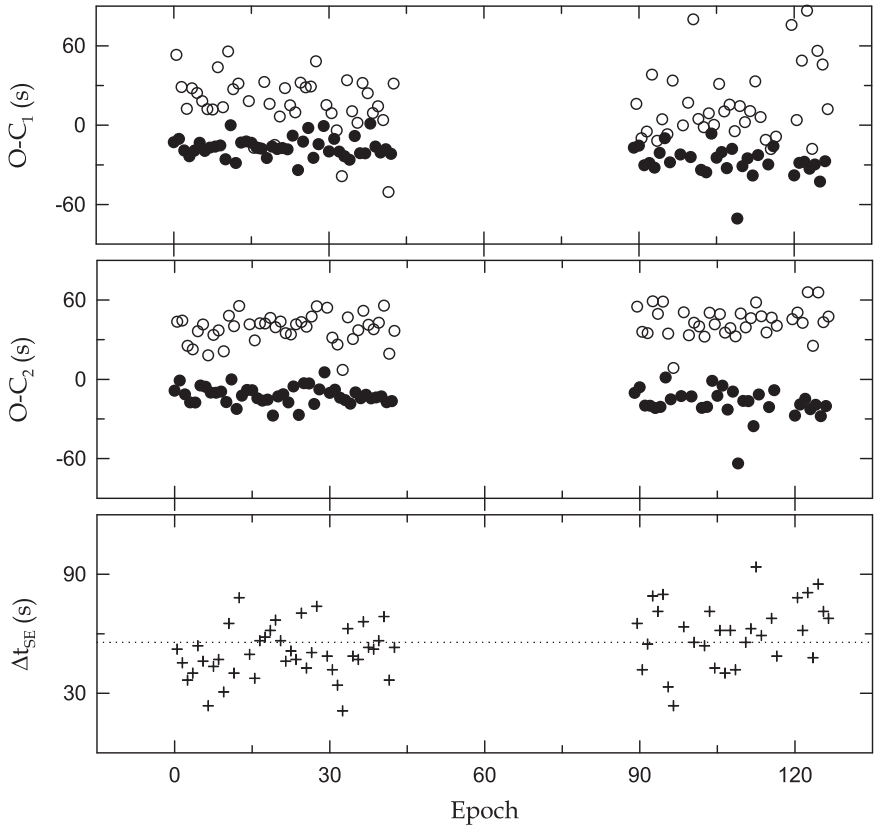

Figure 5. *O–C* diagrams of the minimum times measured from the observed (top panel) and pulsation-subtracted (middle panel) *Kepler* data. The filled and open circles represent the primary and secondary minima, respectively. The bottom panel shows the time delay (Δt_{SE}) of the secondary eclipses related to one half period after the primary eclipses in the pulsation-subtracted data. The dotted line refers to the mean value of $\Delta t_{SE} = 56 \pm 17$ s.

As displayed in Figure 5, the large discrepancy between Min I and Min II is shown more clearly in the pulsation-subtracted data. This discrepancy can result from the time difference between the primary and secondary eclipses due to LTT in a binary with unequal masses (Barlow et al. 2012; Parsons et al. 2014). The Rømer delay is given by Kaplan (2010), as follows:

$$\Delta t_{LTT} = \frac{PK_2}{\pi c}(1 - q), \tag{1}$$

where P is the orbital period, K_2 is the radial velocity (RV) semiamplitude of the secondary star, and c is the speed of light. From the Model 2 parameters in Table 1, we derived the velocities ($K_1 = 13\,\mathrm{km\,s^{-1}}$ and $K_2 = 187\,\mathrm{km\,s^{-1}}$) of the binary components (Hilditch 2001). The time delay of $\Delta t_{LTT} = 34 \pm 1$ s was obtained by applying the values of K_2, P, and q to Equation (1).

In order to examine this possibility, we computed the secondary eclipses related to one half period after the primary eclipses in the pulsation-subtracted data and then plotted the difference (Δt_{SE}) between the measured and computed secondary times in the bottom panel of Figure 5. As shown in the figure, the mean value is offset from zero and gives a time delay of $\Delta t_{SE} = 56 \pm 17$ s in the secondary eclipse. This value is calculated to be $\Delta t_{SE} = 37 \pm 27$ s in the observed *Kepler* data including pulsations. Within their errors, the time delays of Δt_{SE} are in satisfactory accord with the predicted delay of Δt_{LTT}. On the other hand, if KIC 11401845 is in an eccentric orbit, Δt_{SE} might be affected by the time shift of Δt_e in the secondary eclipse due to a nonzero eccentricity:

$$\Delta t_e \simeq \frac{2Pe}{\pi}\cos\omega, \tag{2}$$

$$\Delta t_{SE} \simeq \Delta t_e + \Delta t_{LTT}, \tag{3}$$

where e and ω are the eccentricity and the argument of periastron, respectively. Using Equations (2) and (3), $e\cos\omega \simeq 0.00003$ for the observed data and $e\cos\omega \simeq 0.00019$ for the pulsation-subtracted data.

5. Discussion and Conclusions

We have studied the physical properties of KIC 11401845, based on the *Kepler* data made during Quarters 10 and 12. The light curve of this system displays multiperiodic pulsations, superimposed on binary effects. To examine whether the binary parameters are affected by the pulsations, we analyzed individually the observed and pulsation-subtracted *Kepler* data with the W–D code. As listed in Table 1, the photometric solutions for the two data sets are in good agreement with each other, which means that the pulsations cause little impact on the light-curve parameters. Our light-curve synthesis shows that KIC 11401845 is a short-period detached EB with a very small mass ratio of about 0.07. The primary and secondary components fill $F_1 = 45\%$ and $F_2 = 99\%$ of their limiting lobe, respectively, where the filling factor $F_{1,2} = \Omega_{in}/\Omega_{1,2}$. With its small q and short P, our program target closely resembles the two *Kepler* pulsating EBs KIC 10661783 (Lehmann et al. 2013) and KIC 8262223 (Guo et al. 2016), which are detached binaries with characteristics of the R CMa-type stars (Budding & Butland 2011;

Lee et al. 2016b) among Algols. A comparison of the KIC 11401845 parameters with the mass–radius, mass–luminosity, and Hertzsprung–Russell (H-R) diagrams (İbanoğlu et al. 2006) shows that the primary component resides within the main-sequence band. On the contrary, the low-mass secondary is highly evolved, and its radius and luminosity are remarkably oversized and overluminous compared to main-sequence stars of the same mass. These suggest that the initial more massive star becomes the present secondary by losing most of its own mass via mass transfer to the companion (present primary) and stellar wind (Hong et al. 2015; Guo et al. 2016).

In order to detect the pulsation frequencies of KIC 11401845, multiple-frequency analyses were applied to the out-of-eclipse residuals after removing the binarity effects from the observed *Kepler* data. We found 23 frequencies with S/Ns larger than 4.0 in two regions: 0.4–3.8 day^{-1} and 13.7–23.8 day^{-1}. Among these, four (f_4, f_6, f_9, f_{15}) in the low-frequency region are frequencies at exact multiples of the orbital frequency, $f_{\rm orb} = 0.46267$ day^{-1}. The orbital harmonics can be attributed to tidally excited modes, which occur when the orbital frequency is close to a stellar eigenfrequency in a binary star (Welsh et al. 2011; Hambleton et al. 2013). On the contrary, the other frequencies are strongly reminiscent of the p-mode pulsations known in EBs (e.g., Southworth et al. 2011; Lee et al. 2016b). The ratios of the pulsational to orbital periods in the high-frequency region were calculated to be $P_{\rm pul}/P_{\rm orb} = 0.020$–$0.034$, which is within the upper limit of 0.09 for δ Sct stars in binaries (Zhang et al. 2013). We calculated the pulsation constants by applying the Model 2 parameters in Table 1 to the equation of $\log Q_i = -\log f_i + 0.5 \log g + 0.1 M_{\rm bol} + \log T_{\rm eff} - 6.456$ (Petersen & Jørgensen 1972). The result is listed in the sixth column of Table 2. The Q values of 0.018–0.031 days correspond to p modes of δ Sct type. The period ratios, the pulsation constants, and the position on the H-R diagram reveal that the primary component is a δ Sct variable. The δ Sct pulsations of KIC 11401845 match well the correlations between the pulsation periods and other parameters (binary periods, surface gravities of pulsators, and gravitational forces from companions) updated by Liakos & Niarchos (2017).

We measured the minimum epochs of the primary and secondary eclipses from the observed and pulsation-subtracted data. Inspecting them in detail, we found delays of about 37 and 56 s in the arrival times of the secondary eclipses relative to the primary eclipses in the same order. The values are consistent with the expected time delay of $\Delta t_{\rm LTT} = 34$ s across the binary orbit. This indicates that the LTT delay is the main cause of the time discrepancy between both eclipses, which is the first detection of this effect in EBs consisting of noncompact components. One might imagine that the time delay of the secondary eclipse could be apportioned between the LTT delay and a nonzero eccentricity. The result presented in this paper limits the eccentricity of KIC 11401845 to $e < 0.0002$. When the high-resolution spectra are made, they will help to determine the RV semiamplitudes ($K_{1,2}$) and mass ratio (q) of the binary star and hence to derive its small eccentricity (e). Because the system is a faint pulsating EB with a short orbital period, 8–10 m class telescopes are required to measure its accurate double-lined RVs.

This paper includes data collected by the *Kepler* mission. *Kepler* was selected as the 10th mission of the Discovery Program. Funding for the *Kepler* mission is provided by the NASA Science Mission directorate. We have used the SIMBAD database maintained at CDS, Strasbourg, France. This work was supported by the KASI grant 2016-1-832-01. Work by K.H. was supported by the Basic Science Research Program through the National Research Foundation of Korea (NRF) funded by the Ministry of Education (grant No. NRF-2016R1A6A3A01007139).

References

Barlow, B. N., Wade, R. A., & Liss, S. E. 2012, ApJ, 753, 101
Borucki, W. J., Koch, D., Basri, G., et al. 2010, Sci, 327, 977
Breger, M. 2000, in ASP Conf. Ser. 210, Delta Scuti and Related Stars, ed. M. Breger & M. H. Montgomery (San Francisco, CA: ASP), 3
Breger, M., Stich, J., Garrido, R., et al. 1993, A&A, 271, 482
Budding, E., & Butland, R. 2011, MNRAS, 418, 1764
Gaulme, P., & Guzik, J. A. 2014, in Proc. IAU Symp. 301, Precision Asteroseismology, ed. J. A. Guzik et al. (Cambridge: Cambridge Univ. Press), 413
Guo, Z., Gies, D. R., Matson, R. A., et al. 2016, ApJ, submitted (arXiv:1610.00350)
Hambleton, K. M., Kurtz, D. W., Prša, A., et al. 2013, MNRAS, 434, 925
Harmanec, P. 1988, BAICz, 39, 329
Hilditch, R. W. 2001, An Introduction to Close Binary Stars (Cambridge: Cambridge Univ. Press)
Hong, K., Lee, J. W., Kim, S.-L., et al. 2015, AJ, 150, 131
İbanoğlu, C., Soydugan, F., Soydugan, E., & Dervişoğlu, A. 2006, MNRAS, 373, 435
Kallinger, T., Reegen, P., & Weiss, W. W. 2008, A&A, 481, 571
Kaplan, D. L. 2010, ApJL, 717, L108
Kepler Mission Team 2009, yCat, 5133, 0
Kirk, B., Conroy, K., Prša, A., et al. 2016, AJ, 151, 68
Koch, D. G., Borucki, W. J., Basri, G., et al. 2010, ApJL, 713, L79
Koo, J.-R., Lee, J. W., Lee, B.-C., et al. 2014, AJ, 147, 104
Kreiner, J. M., Kim, C.-H., & Nha, I.-S. 2001, An Atlas of O–C Diagrams of Eclipsing Binary Stars (Krakow: Wydawn. Nauk. Akad. Pedagogicznej)
Kwee, K. K., & van Woerden, H. 1956, BAN, 12, 327
Lee, J. W. 2016, ApJ, 833, 170
Lee, J. W., Hong, K., Kim, S.-L., & Koo, J.-R. 2016a, MNRAS, 460, 4220
Lee, J. W., Kim, S.-L., Hong, K., et al. 2016b, AJ, 151, 25
Lee, J. W., Kim, S.-L., Hong, K., Lee, C.-U., & Koo, J.-R. 2014, AJ, 148, 37
Lehmann, H., Southworth, J., Tkachenko, A., & Pavlovski, K. 2013, A&A, 557, A79
Lenz, P., & Breger, M. 2005, CoAst, 146, 53
Liakos, A., & Niarchos, P. 2015, in ASP Conf. Ser. 496, Living Together: Planets, Host Stars and Binaries, ed. S. M. Rucinski, G. Torres, & M. Zejda (San Francisco, CA: ASP), 195
Liakos, A., & Niarchos, P. 2016, arXiv:1606.08638
Liakos, A., & Niarchos, P. 2017, MNRAS, 465, 1181
Loumos, G. L., & Deeming, T. J. 1978, Ap&SS, 56, 285
Mkrtichian, D. E., Kusakin, A. V., Rodriguez, E., et al. 2004, A&A, 419, 1015
Murphy, S. J., Shibahashi, H., & Kurtz, D. W. , 2013, MNRAS, 430, 2986
Parsons, S. G., Marsh, T. R., Bours, M. C. P., et al. 2014, MNRAS, 438, L91
Petersen, J. O., & Jørgensen, H. E. 1972, A&A, 17, 367
Rodríguez, E., & Breger, M. 2001, A&A, 366, 178
Southworth, J., Zima, W., Aerts, C., et al. 2011, MNRAS, 414, 2413
Torres, G. 2010, AJ, 140, 1158
Torres, G., Andersen, J., & Giménez, A. 2010, A&ARv, 18, 67
Van Hamme, W. 1993, AJ, 106, 209
Van Hamme, W., & Wilson, R. E. 2007, ApJ, 661, 1129
Welsh, W. F., Orosz, J. A., Aerts, C., et al. 2011, ApJS, 197, 4
Wilson, R. E., & Devinney, E. J. 1971, ApJ, 166, 605
Zhang, X. B., Luo, C. Q., & Fu, J. N. 2013, ApJ, 777, 77